Optics and Lasers in Engineering 121 (2019) 261–270

Contents lists available at ScienceDirect

Optics and Lasers in Engineering

journal homepage: www.elsevier.com/locate/optlaseng

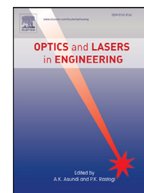

Optical measurement of surface topographies with transparent coatings

Xiaobing Feng[a,b,*], Nicola Senin[b,c], Rong Su[b], Suresh Ramasamy[d], Richard Leach[b]

[a] State Key Laboratory of Mechanical System and Vibration, School of Mechanical Engineering, Shanghai Jiao Tong University, Shanghai, China
[b] Manufacturing Metrology Team, University of Nottingham, Nottingham, UK
[c] Department of Engineering, University of Perugia, Perugia, Italy
[d] Apple Inc., California, USA

ARTICLE INFO

Keywords:
Optical measurement
Surface topography
Surface metrology
Transparent coating

ABSTRACT

Manufacturers nowadays have access to state-of-the-art areal surface topography measurement instruments that allow investigation of surface topography at unprecedented levels of detail and over a wide range of scales. However, high value-added products have demanding requirements, pushing measurement technologies to their limits. Therefore, a deeper insight and more comprehensive understanding of performance and behaviour of current areal surface topography measurement solutions is often needed. In this work, we investigate and compare the results when measuring the same surface with different, state-of-the-art areal surface topography measurement solutions involving the principal optical technologies, notably focus variation microscopy, coherence scanning interferometry, imaging confocal microscopy and point autofocus instrument, operated using different set-ups. The test case is a highly engineered surface obtained through a sequence of mechanical and chemical surface modification processes. The surface has complex topographic formations at micrometre and sub-micrometre scales, and is characterised by the presence of a thin transparent layer, notoriously challenging for optical measurement. The topographies reconstructed from measurement are compared both in terms of visual appearance and texture parameters.

1. Introduction

Surface engineering is increasingly applied to improve manufactured products, adding value to various aspects such as performance, durability and aesthetics [1]. Applications include optimising aeroplane windshield and turbine blade surfaces to repel high-speed water drops [2], improving electrocatalysis efficiency of fuel cells for transportation applications [3], tailoring the surface roughness of scaffolds for skeletal tissue regeneration [4], enhancing cavitation corrosion resistance of engineering components such as mechanical heart valves and ship propellers [5] and developing consumer products with more appealing 'look and feel' to attract consumers [6]. To achieve the specified surface properties, surfaces are often subjected to advanced mechanical, thermal and chemical modification processes [5,7,8]. Quality control for these modification processes often pushes areal surface topography measurement to its limits. In such demanding scenarios, a better understanding of how the measurement instruments operate is necessary in order to better utilise them to capture the signatures of the topography modification processes.

A wide range of measurement technologies is available to capture surface topographies with features at micrometre and sub-micrometre scales [9]. The ISO 25178 series [10–16] of specification standards has been created for areal surface topography measurement, with ISO/FDIS 25178-600 [15] describing nominal metrological characteristics of areal surface topography measurement instruments and ISO/CD 25178-700 [16] describing the calibration and verification of the instruments. Areal surface topography measurement instruments are individually described in the ISO 25178-60x series and their calibration has been investigated in several studies [17–25]. Covered technologies include contact stylus [10,19], imaging confocal microscopy (ICM) and chromatic confocal microscopy [11,19,20,26], phase shifting interferometry [25] and coherence scanning interferometry (CSI) [12,18–20], point autofocus instruments (PAI) [13,23] and focus variation microscopy (FVM) [14,24,27]. The methods suggested in the ISO 25178 series to characterise the metrological performance of the measurement technologies require the use of calibrated material measures [9,15,17], which typically have relatively simple geometries, such as flat surfaces and step height features. As a result, such methods cannot accurately characterise the behaviour

* Corresponding author at: Shanghai Jiao Tong University, Room A728, Mechanical Engineering Building No. 800 Dongchuan Road, Shanghai 200240, China.
E-mail address: xiaobing.feng@sjtu.edu.cn (X. Feng).

https://doi.org/10.1016/j.optlaseng.2019.04.018
Received 30 January 2019; Received in revised form 26 March 2019; Accepted 23 April 2019
Available online 29 April 2019
0143-8166/© 2019 The Authors. Published by Elsevier Ltd. This is an open access article under the CC BY license. (http://creativecommons.org/licenses/by/4.0/)

of instruments when dealing with challenging materials with complex optical properties, surfaces subjected to a sequence of modification processes and surfaces with complex and highly irregular topographies [28]. In such scenarios, evaluation of the task-specific characteristics of the instruments (i.e. how the instruments behave when operating in specific application scenarios) needs to be carried out.

Comparisons of different instruments for surface topography measurement often show widely-varying results, especially with complex surfaces; see for example [29,30]. Leach et al. [17,31] have investigated the methods and material measures involved to compare the performance of various areal surface topography measuring instruments. de Groot et al. [22] have looked into issues involved when comparing measurement noise of instruments with different measurement bandwidth and speed.

The test case investigated in this work consists of the surface of a high-end technology consumer product featuring complex topographic formations at micrometre and sub-micrometre scales. The surface is characterised by the presence of a thin transparent layer, notoriously challenging for optical measurement due to its transparency and reflectance characteristics [32–34]. The surface is measured with state-of-the-art instruments implementing a number of commercially available optical technologies for areal topography measurements, notably FVM, ICM, CSI and PAI, and using different instrument set-ups. The selected test case represents the type of surfaces involved in a variety of applications in the consumer industry such as electronics, sports goods and interior design. It is representative of a typical scenario often encountered when dealing with the characterisation of highly engineered products; where innovation advances at a fast rate, there are no suitable calibrated material measures available [28]; and often there are no appropriate reference measurement technologies with task-specific estimations of uncertainty. In the case of the selected surface, existing calibrated thin film references do not sufficiently reflect the challenges presented by the complex topographic formations on the surfaces.

In this work, it is shown how, in the above-mentioned circumstances, it is still possible to understand important aspects of how each instrument operates by comparative assessment of geometric reconstructions of surface topography obtained from the measured data. The proposed comparison offers a qualitative perspective, based on visual inspection of reconstructed models, and a quantitative perspective, obtained via computation of texture parameters (ISO 25178-2 areal texture parameters [35,36]). Before texture parameters can be compared, the topographic datasets obtained by measurement are relocated (i.e. co-localised in space) and laterally trimmed to ensure matching boundaries, in order to guarantee that each computed texture parameter refers to the same region on the original surface.

Due to the lack of an external, more accurate reference to compare results to, the assessment of measurement performance and behaviour can only rely on consensus, i.e. multiple datasets showing closeness of results. However, relying on consensus is not intrinsically robust, because multiple instruments or set-ups could agree on an inaccurate result. Such a risk can be reduced by increasing the number of sources of information. For the application presented in this work, additional sources of information on one or both of the layers have been selected in the form of optical microscope imaging with focus stacking (FS), scanning electron microscopy (SEM), and atomic force microscopy (AFM). It is important to point out that none of these additional sources of information can necessarily be considered as more accurate than the optical solutions being investigated (FVM, CSI, PAI and ICM). Thus, none of them can act as a traceable comparison reference—to the authors' knowledge, such a reference is not available. Moreover, whilst AFM produces areal topography datasets which can be turned into geometric models that are at least quantitatively comparable with those produced by the investigated optical solutions, both SEM and FS can only produce images, whose usefulness is limited to the assessment of topographic properties on the image plane. Regardless, such additional sources of information contribute to increase the number of sources that are assessed for consensus, thus intrinsically increasing the robustness of the method.

2. Methodology

2.1. Test case

The test case consists of a metallic surface featuring complex topographic formations at micrometre and sub-micrometre lateral and height scales, and is characterised by the presence of a transparent layer of unknown thickness. The surfaces have been produced from a sequence of proprietary chemical and mechanical modification processes; further details of these processes cannot be given for commercial reasons.

2.2. Sample preparation and surface topography measurement

Before being measured, the sample surface was subjected to fabrication of fiducial marks by indentation (Buehler 1600–6400 microhardness tester, with a Vickers indenter and 1.96 N load), and then cleaned in an ultrasonic bath (Shesto UT8031) for ten minutes in distilled water at room temperature.

The sample surface was measured via SEM and FS. Areal topography data was obtained via AFM, FVM, PAI, ICM and CSI. The sequence of observation was: SEM and FS; then FVM, PAI, ICM, AFM and CSI.

Measurement settings used with the four evaluated technologies are listed in Tables 1–4, respectively. Measurement settings used with AFM

Table 1
Measurement settings used with FVM.

Magnification	20×	50×	100×
Sampling distance / µm	0.44	0.18	0.09
Field of view / mm	0.8 × 0.8	0.32 × 0.32	0.16 × 0.16
Illumination type	Co-axial		
Illumination wavelength	Broad band (white)		
Estimated vertical resolution / nm	26	11	4
Exposure time / ms	0.075	0.242	0.394
Contrast	0.65	1.01	0.81

Table 2
Measurement settings used with PAI.

Objective magnification	100×	Sampling distance / µm	0.1
Laser wavelength / nm	635	Vertical resolution / nm	1
Laser spot size / µm	1	Sampling mode	Index
Numerical aperture	0.8	Autofocus sensor	Select, wide
Working distance / mm	3.4	Autofocus gain	Standard

Table 3
Measurement settings used with ICM.

Magnification	50×	100×
Illumination wavelength / nm	405	
Vertical resolution / nm	10	
Numerical aperture	0.95	
Sampling distance / µm	0.25	0.13
Field of view / mm	0.25 × 0.25	0.12 × 0.12

Table 4
Measurement settings used with CSI.

Magnification	20×	50×
Illumination wavelength	Broad band (white)	
Vertical resolution / nm	0.005	
Zoom	1×	1×
Field of view / mm	0.43 × 0.43	0.17 × 0.17
Sampling distance / µm	0.43	0.17
Numerical aperture	0.40	0.55
Oversampling function	Enabled	Enabled

Table 5
Measurement settings used with AFM.

Operating mode	Tapping mode	Sampling distance / µm	0.16
Amplitude setpoint / V	0.25	Raster frequency / Hz	0.2
Field of view / mm	0.06 × 0.06	Z-axis travel range / µm	6.8

are listed in Table 5. Measurement settings involved in focus stacking imaging (FS) using a digital optical microscope with epi-illumination are listed in Table 6. Focus stacking for the FS measurement was performed using the Zerene Stacker software with 'PMax' mode, which is an implementation of the pyramid method for image data processing [37]. Measurement settings used with SEM imaging are listed in Table 7. Given that the surface was found to be electrically non-conductive, the SEM was operated in low pressure mode. Vertical resolution of the evaluated instruments (FVM, PAI, ICM and CSI) are also listed in the tables to provide reference to the axial sensitivity of the instruments. In the case of FVM, the estimated vertical resolution is not set by the user, but instead provided by the instrument software as a result of measurement settings, the obtained data and the signal analysis algorithm. Vertical resolution of PAI is the resolution of the linear scale in the vertical axis. Vertical resolution of ICM is provided by the manufacturer. Vertical resolution of CSI is defined as the repeatability of the root mean square (RMS) of the surface height, i.e. texture parameter *Sq*. Given that the evaluated instruments operate on different working principles and that vertical resolution is defined differently in each case, the vertical resolution values listed in the tables are not suitable for direct comparison of the performance of the instruments based on different technologies, but serve only as a reference for the readers using the same type of instrument.

Because the surface features are expected to range from a few micrometres to tens of micrometres in the lateral scale, measurement settings, such as magnification and field of view (FoV), were selected in order to achieve sub-micrometre lateral sampling spacing [29,30]. Because of the optical challenges posed by the native surface to the FVM technology (essentially because of lack of contrast in imaging, see Section 3.3), a silicone-based replica product (AccuTrans) was used to replicate the sample surface.

A preliminary assessment of the thickness of the transparent layer was performed in order to have additional information useful to better assess the quality of the subsequent optical topography measurements. Film thickness was obtained by using the following method. CSI was adopted, with film measuring mode enabled. The thickness measuring instrument has been previously verified using a thin film material measure [38]. A vertical scan was performed across a range of 40 µm, chosen under the assumption that it would approximately encompass both the top and substrate surfaces. During film thickness measurement, the illuminating light was reflected as well as scattered by both the top surface and the substrate surface. Light reflected/scattered from both surfaces interfered with the reference beam, resulting in two interference signals corresponding to the two surfaces (see Fig. 3). The optical distance between the two surfaces was determined by the peak positions of the interference signals using methods such as envelope detection and frequency domain analysis [39,40]. The optical distance was subsequently divided by the refractive index of the transparent layer to obtain the layer thickness. While a higher magnification (50×) is preferred in surface topography measurement, layer thickness measurement was performed at 20× magnification in order to assess the layer thickness over a larger area.

Table 7
Imaging settings used with SEM.

Electron source	Tungsten filament	Accelerating voltage / kV	10
Pressure mode	Low pressure	Magnification	1000×
Detector type	Backscattering	Imaging mode	Shadow

2.3. Data analysis and processing

The areal topography datasets obtained by AFM, FVM, PAI, ICM and CSI were pre-processed with the surface metrology software MountainsMap [41] to perform: (i) filling of non-measured points by interpolation of valid neighbours, (ii) removal of outlier points, and (iii) levelling by subtraction of the least-squares mean plane.

All the areal topography datasets taken from the same region of a surface were relocated (i.e. co-localised within the same co-ordinate system), using the AFM dataset as the alignment reference. Non-overlapping portions located at the sides of each dataset were trimmed out, in order to ensure that any quantitative assessment would include the same region of topography.

Relocation (i.e. alignment) of measured topography datasets was performed using a custom method developed by the authors and implemented in Matlab. Firstly, height maps were converted to triangulated meshes, so that alignment could be conducted in six degrees of freedom. Secondly, coarse alignment of measured topographies was performed through an iterative procedure consisting of applying manual adjustments (translations and rotations), using the fiducial marks as reference landmarks for alignment. The iterative procedure is based on a continuous assessment of residual misalignment, computed as the RMS of the distances between paired vertices in the two triangulated meshes being aligned. Thirdly, a further, fine alignment process was performed via iterative closest points [42]. The same misalignment metric was used in coarse and fine alignment. Lastly, aligned meshes were turned back into height maps via raster scanning (i.e. by projecting a pattern of rays along the z-direction onto the meshes and computing the intersections). All the measured topographies were aligned to the same reference measurement (AFM dataset), and cropped to the largest rectangle fully inscribed within the overlapping area.

Bandwidth matching of the aligned topographies was not performed. In bandwidth matching, band-pass filters are applied to all the datasets in order to ensure that the same range of spatial wavelengths is represented by all the measurements, so that the comparison can focus on the different behaviour the measurement technologies have over topographic features acquired within the same range of scales [31]. In this work, however, it was deemed interesting to compare measurement technologies also in terms of their different capabilities of capturing features at different scales, thus bandwidth matching was not applied.

Quantitative assessment and comparison was performed by computation of the ISO 25178-2 field areal texture parameters: *Sa, Sq, Sal, Sku* and *Ssk* [35], applied to the aligned topography datasets to make sure that the parameters would not be affected by features included in one dataset but missing in another just because of different region coverage.

3. Results

3.1. Visual assessment from SEM and optical FS

Fig. 1 shows how the same surface region appears when imaged by SEM at 1000× and by optical microscopy at 100×, in FS mode. One

Table 6
Imaging and processing settings used with FS.

Magnification	100×	Numerical aperture	0.8
Illumination type	Co-axial	Image stack size	81
Exposure time / ms	0.394	Vertical scanning range / µm	40
Sampling distance / µm	0.09	Image stacking software	Zerene stacker
Field of view / mm	0.14 × 0.11	Image stacking method	PMax

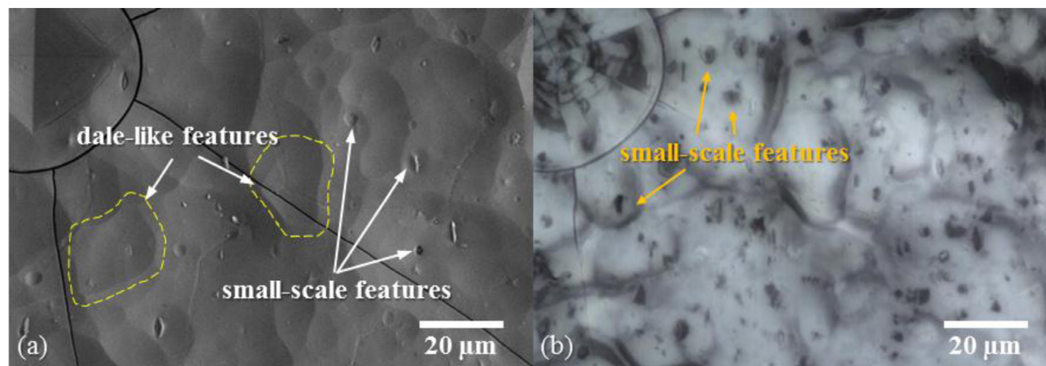

Fig. 1. Image of the sample surface obtained (a) by an SEM at 1000× magnification and (b) by an optical microscope with at 100× magnification with focus stacking. An indentation mark is located at the top-left corner of the images.

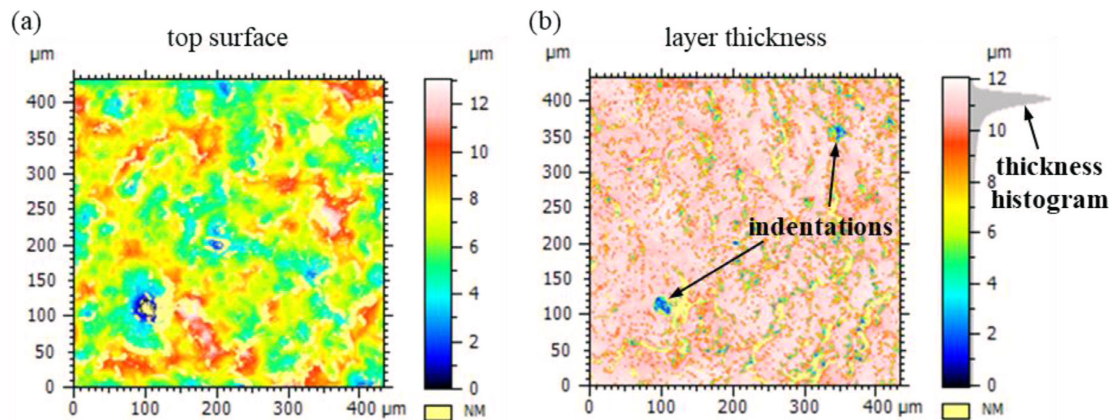

Fig. 2. (a) Surface topography of the top surface and (b) map of local film thicknesses as computed from the difference of the top surface and substrate topography maps (CSI used in film measurement mode).

of the indentation marks used for co-localisation, and its surrounding cracks (due to the indentation process) are visible in the top-left corner. Patterns of topologically connected, dale-like surface features dominate the surface with lateral scales approximately ranging from tens of micrometres to a few micrometres. Two example dale-like features are illustrated with yellow dashed contours in Fig. 1(a). The contours are slightly shifted outwards so that the underlying topography ridges are visible. Additional, smaller-scale features were often observed, either in the form of pits, or in the form of protrusions, in both cases usually at least one order of magnitude smaller than the dale-like feature within which they appeared. Both the pit-like and the protruded singularities are referred to as “small-scale” features from now onwards. The optical images revealed an increased number of small-scale features with respect to what was observable by SEM. This is likely due to fact that the vertical scanning range in FS encompassed both the top and substrate surfaces, thus revealing surface features both on and between the surfaces. It is also possible that some surface features were revealed with better contrast under an optical microscope than in an electron microscope. Most of such additional small-scale features would be distinguishable by colour in the FS dataset. Conversely, the partitioning into dale-like features, evident from the SEM images, was not found as consistently in the optical FS dataset, possibly because of being masked by the chromatic patterns visible on the surface. By simple visual inspection of the SEM and FS images, it is unclear whether the dale-like patterns belong to the substrate, the transparent layer, or both.

3.2. Transparent layer thickness

Fig. 2 shows the results of the CSI measurement of a region of 0.43 mm × 0.43 mm performed to estimate the film thickness. As the measurement was performed in film measurement mode, one of the results of the procedure is an estimation of the topographies of both the top surface and the substrate. In Fig. 2(a) the top surface is shown, whilst in Fig. 2(b) the substrate surface (height map) has been subtracted from the top surface (also a height map) to obtain a map of local thickness values (shown in the figure). In the thickness map, two indentation marks present in the measured region are partially visible as regions where thickness decreases towards zero. The frequency distribution of thickness values is shown in histogram form next to the colour scale in Fig. 2(b). It can be seen that layer thickness is relatively uniform in most measurable regions (i.e. apart from the indentation marks and regions where local surface slopes are beyond the numerical aperture slope limit of the objective lens). The mean thickness distribution was computed as 11.3 µm.

A closer look at the same area as in Fig. 1 is given in Fig. 3. The indentation mark is located at the top left corner of the image. The top-view intensity map (in the *x*-*y* plane) of the top surface as obtained from CSI measurement is shown in Fig. 3(a). A cross-sectional slice (in the *x*–*z* plane) of the 3D CSI signal data is shown in Fig. 3(b). The location where this slice is taken is marked in Fig. 3(a). The interference fringes in Fig. 3(b) carry the location information of the top and substrate surfaces. The interference signals corresponding to the substrate surface were weaker than those corresponding to the top surface. Therefore, in Fig. 3(b), image contrast was enhanced in the region containing the substrate surface for visual clarity. The low signal intensity at the substrate surface may be due to the roughness of the substrate surface and absorption of the transparent layer. It can be observed that the form of the substrate surface qualitatively followed that of the top surface, confirming that the transparent layer is relatively uniform in thickness. Fig. 3(c) shows the intensity of the interference signal at one

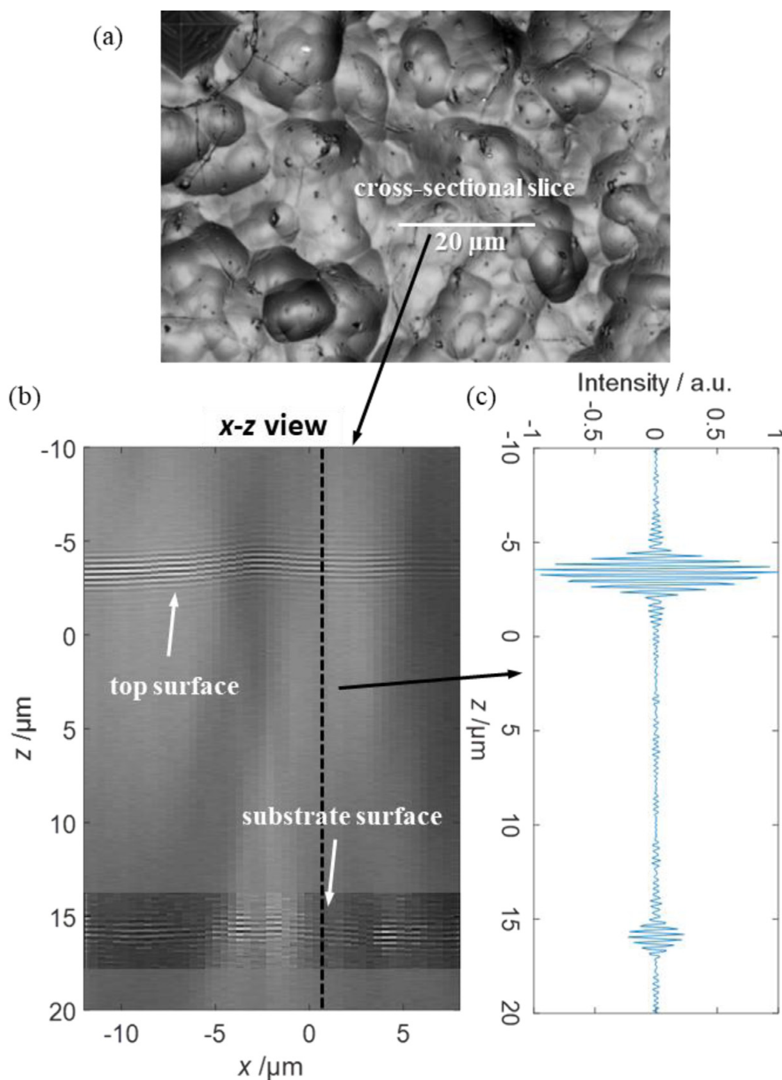

Fig. 3. CSI signals of the film measurement. (a) Top-view intensity map of the measured area in the x-y plane, (b) an arbitrarily-chosen cross-sectional slice through 3D CSI signals, and (c) interference signal at a single point on the surface along the z-axis (signal intensity is expressed in arbitrary units normalised to one).

surface point (a specific x and y position) on the profile. The signal was band-pass filtered to remove the background intensity [43]. Signal intensity in the substrate surface was observed to be significantly weaker than in the top surface. The signal to noise ratio at certain regions (e.g. with high surface slope) on the substrate surface would sometimes be lower than required to correctly identify the substrate surface, which contributed to non-measured points (represented in yellow) in Fig. 2(b). The layer thickness was determined based on the assumption that the refractive index value remains constant across the measured area. Any fluctuations in the local refractive index value would result in errors in the thickness distribution. Other contributors to errors in the layer thickness measurement include (1) the relatively low signal to noise ratio in the interference signals from the substrate surface and (2) measurement artefacts, the impact of which will be discussed further in Section 3.3.

3.3. Areal topography measurements with optical instruments

Example results are presented in the following sections, pertaining to a single region of the sample, as measured via AFM, FVM, PAI, ICM and CSI. The region selected for illustration is the same as that previously used in Fig. 1.

3.3.1. Focus variation microscopy

Surface topographies measured at 20×, 50× and 100× magnification are shown in Fig. 4(a), (b), and (c). The 20× and 50× datasets were cropped to the same FoV as those measured at 100× magnification. As the region is the same as in Fig. 1, the same indentation mark was also observed at the top corner of the topographies (barely visible in Fig. 4). The main issues encountered with FVM measurement were: the different optical properties of the two surfaces, the top surface being transparent, the substrate being more reflective, leading to issues in the identification of optimal illumination conditions; lack of textural detail in particular at high magnifications, leading to poor contrast detection; and the two surfaces being close enough to each other to present overlapping ranges of focal distances, often misleading the instrument into focusing onto the wrong one. The irregular and plateau-shaped topographies shown in Fig. 4(a)–(c) are indicative of FVM possibly jumping back and forth between the top surface of the transparent layer and the surface of the substrate, depending on local contrast detection, and also attempting to find a solution based on resolved height values for neighbouring points, leading to the plateau effect observed in previous work [44]. The percentage of non-measured points (i.e. points that the instrument itself recognises as unmeasurable, because of lack of information) in the same region was found to increase with magnification, as shown in Table 8. Since FVM relies on computation of local image contrast to determine surface local height values, lowered image contrast in local areas resulting from higher magnifications was deemed as one of the main causes of increased percentage of non-measured points. With polarised light, the number of non-measured points was significantly reduced, as shown in Fig. 4(d) and Table 8, albeit the reconstructed topographies still showed signs consistent with jumping between two layers.

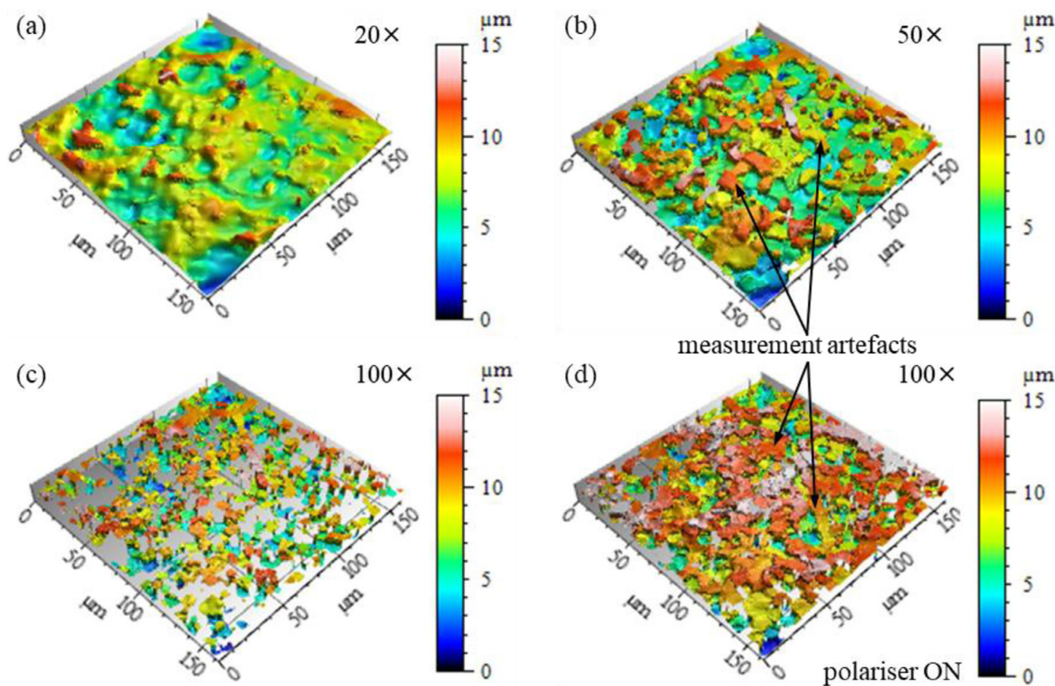

Fig. 4. Surface topographies measured by FVM without using a polarising filter: (a) at 20× magnification, (b) at 50× magnification, (c) at 100× magnification; and (d) surface topography measured at 100× magnification using a polarising filter.

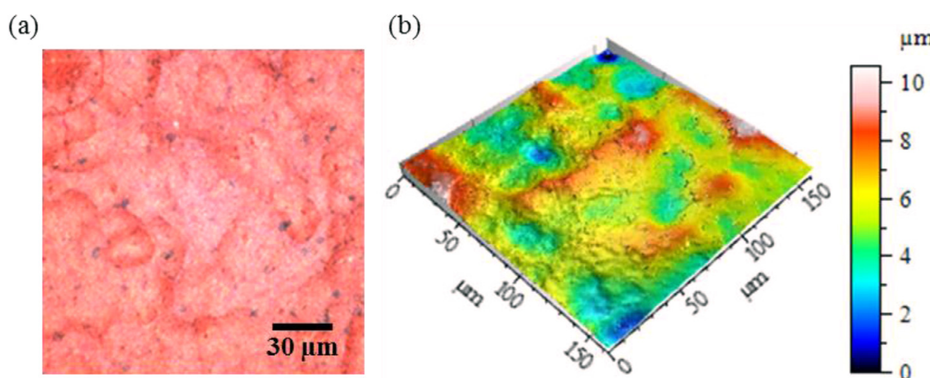

Fig. 5. Replicated sample surface: (a) full-focus RGB map obtained by FVM (b) FVM surface topography measured at 100× magnification. Both the RGB and the height map were corrected for the mirror effect (i.e. the physical replicate containing a specular version of the actual topography, with inverted axes).

Table 8
Percentage of non-measured points in topographies measured at various magnification and polarisation using FVM.

Magnification	20×	50×	100×	100× polarised
Percentage of non-measured points	0.02%	1.89%	37.3%	9.85%

To overcome the issues with contrast detection, the sample surface was replicated using the AccuTrans material (as mentioned in Section 2.2.), a special-purpose silicone filled with microscopic particles designed to enhance contrast [45]. Of course, this approach implies that only the top surface of the sample can be measured. The height map (reconstructed surface topography) and colour map overlay obtained by FVM measurement of the replicate surface are shown in Fig. 5. The indentation mark is visible at the top-left corner of the microscope image, and at the top corner of the height map. Thanks to the use of replication, the measured surface topography was significantly improved. However, an additional medium-scale waviness component (several micrometres in size) was observed on the topography measured with this technique (not visible in Fig. 5), which had not previously been observed in the SEM and FS images.

3.3.2. Point autofocus instrument

The PAI instrument operates using the beam-offset method [9]. The two setting variants used in the study are ‘select’ and ‘wide’, which affect the size of the autofocus detector area utilised to capture the reflected laser beam. The ‘wide’ option uses a larger detector area in order to provide better tracking for surfaces with sudden height shifts (e.g. rough surfaces). The ‘select’ option enables the instrument to automatically choose the optimal detector area during measurement based on the type of surface being measured. Measured topographies using both options are shown in Fig. 6. The indentation mark is still located at the top left corner of the height maps. In the topography measured with the ‘select’ option, a few regions protruding from the rest of the surface were observed. The height of the protrusions is consistent with the thickness of the transparent layer determined in Section 3.2, suggesting that in those locations the instrument may have shifted from measuring the substrate to measuring the top surface of the transparent layer. This transition was not observed when using the ‘wide’ option, however, a higher degree of, what would seemingly appear as, noise was observed. In both PAI configurations, an additional type of artefact was observed on the measured topography in the form of streaks oriented along the scanning direction, which has been determined as a result of the drift compensation function in the instrument software [23].

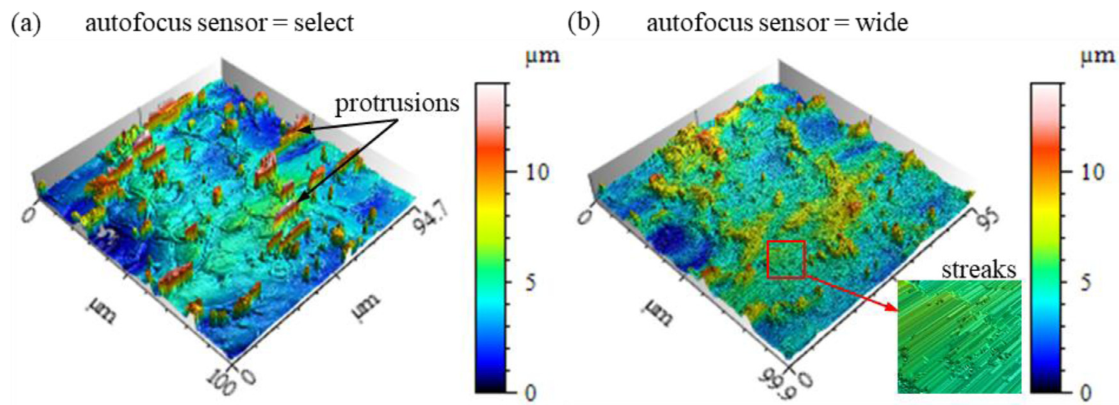

Fig. 6. Surface topographies measured by PAI with autofocus (AF) sensor in (a) 'select' and (b) 'wide' mode.

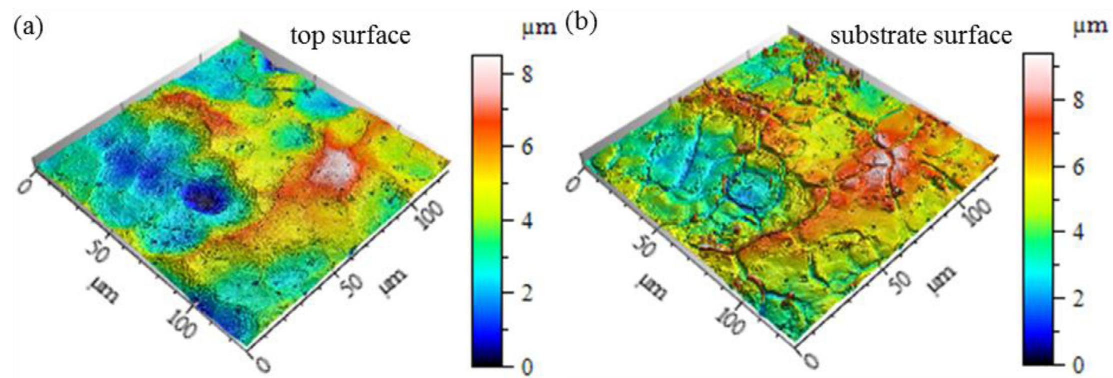

Fig. 7. Surface topographies measured by ICM at 100×: (a) top surface and (b) substrate surface.

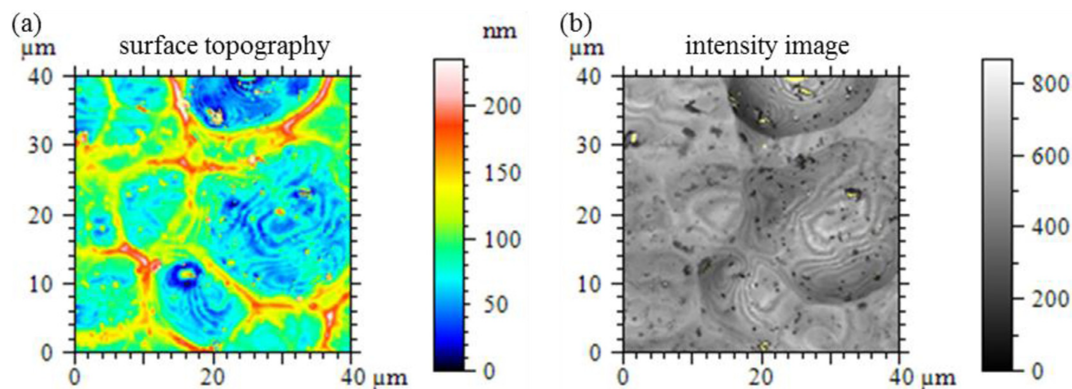

Fig. 8. A sample surface measured by ICM at 100× magnification: (a) surface topography and (b) intensity image.

3.3.3. Imaging confocal microscopy

The ICM instrument allowed measurement of both the top surface and the underlying substrate separately by focusing the instrument on the top surface and substrate respectively. The imaged region was small enough to reduce the risk of the selected surface being replaced by the other as a consequence of going out of vertical scanning range. Measured topographies of the top surface and the substrate surface at 100× magnification are shown in Fig. 7. In the reconstructed topographies shown in Fig. 7, the indentation mark is located at the top corner of the topographies. No significant noise or artefacts were observed on the top surface in Fig. 7(a). The topography of the substrate surface appeared to share a similar topographic pattern with the top surface. However, trenches up to approximately 2.5 µm deep were found on the substrate surface topography at locations that coincide with ridges on the top surface. This coincidence suggests that the presence of a transparent layer with varying surface slope angles may have interfered with the measured depth of the substrate surface.

The presence of a transparent layer on top of the substrate also created minor measurement artefacts on the top surface, as shown in Fig. 8. The artefacts appeared in the form of concentric contour lines whose locations and forms were in good agreement with the contour lines observed in the intensity image. It is likely that light reflected from both the top and substrate surfaces form an interference pattern, causing errors in the intensity signal that is used to determine surface height. Height variation up to approximately 15 nm peak-valley magnitude were observed in the topography. The magnitude of height variation was determined by (i) extracting profiles across the contour lines, (ii) applying a Gaussian filter with 2.5 µm cut-off, and (iii) computing the peak-valley magnitude of the resulting high-pass profile.

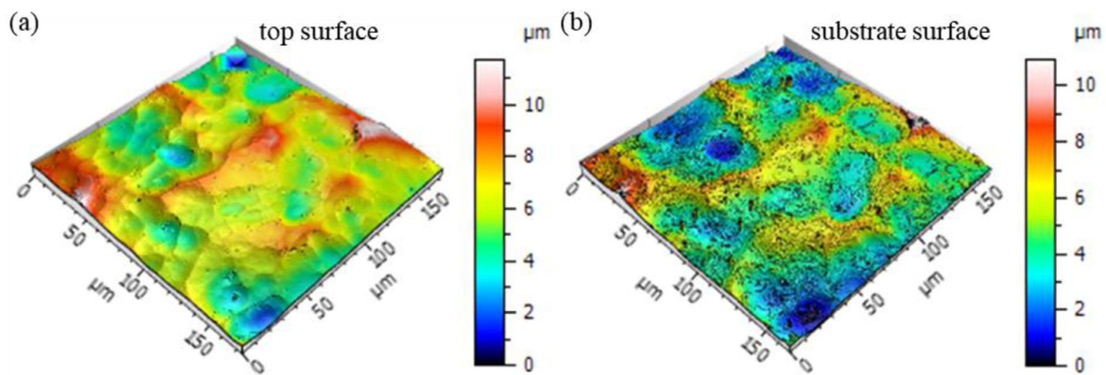

Fig. 9. Surface topographies measured by CSI at 50×: (a) top surface and (b) substrate surface.

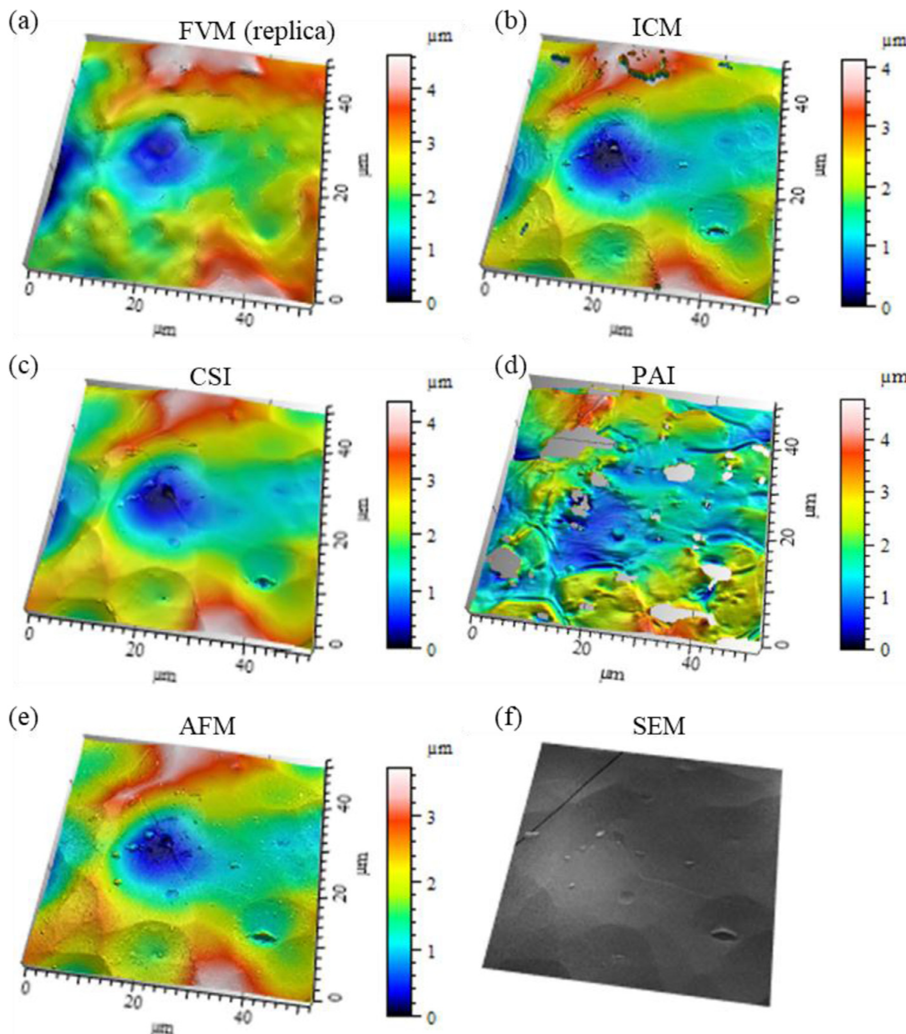

Fig. 10. Surface topographies aligned for comparison: (a) replicated surface measured by FVM at 100× magnification, (b) sample surface measured by ICM at 100× magnification, (c) sample surface measured by CSI at 50× magnification, (d) sample surface measured by PAI with 0.1 μm sampling distance, (e) sample surface measured by AFM with 0.16 μm sampling distance and (f) sample surface image by SEM at 1000× magnification.

3.3.4. Coherence scanning interferometry

Surface topography was measured at 50× magnification to achieve the highest lateral resolution available and improve measurement where high surface slope angle is present. Measured topographies of the top surface is shown in Fig. 9(a). The indentation mark is located at the top corner of the height map. The contour artefacts found in the topography measured by ICM (Fig. 8) are not noticeable in the topography measured with CSI. In addition, the height map of the substrate surface, reconstructed as the difference between the top surface and the thickness of the transparent layer, is shown in Fig. 9(b). Non-measurement points in the substrate surface are mainly due to void data in the layer thickness measurement. The trenches found near the ridges in Fig. 7(b) were not observed.

3.4. Visual comparison of optical areal topography measurements with SEM and AFM data

Topographic details from the top surface measured by the four evaluated technologies (FVM, CSI, ICM and PAI) are shown in Fig. 10, along with a reference topography measured by AFM and an SEM image of

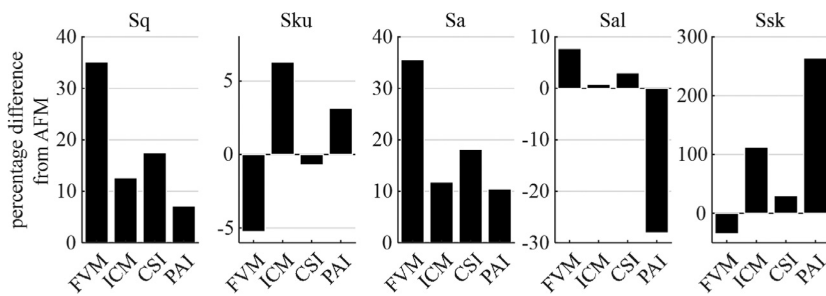

Fig. 11. Percentage difference of values of areal texture parameters computed using topographies measured by FVM, ICM, CSI and PAI. Areal texture parameters computed on AFM data are used as the reference.

the same region (two-dimensional, but shown tilted to facilitate visual comparison). The topographies were aligned and cropped to the same extents as described in Section 2.3. In the case of FVM, the measurements from the silicone replica sample were used.

From the analysis of all the datasets reported in Fig. 10, a few observations can be made. For FVM, the most visible issue was the limited capability to replicate small-scale surface features, a limitation hinted at in Section 3.3.1, presumably due to the physical limitation of the silicone replica production process. ICM appeared to have the highest lateral resolution, as may be expected [46]. CSI had slightly lower lateral resolution, but this is sufficient to retain most of the topographic detail of the surface. In the case of PAI, the most notable issue was what seemed to be a continuous alternation between the capture of the top and substrate surfaces.

3.5. Quantitative comparison via texture parameters

To compare the measured topographies quantitatively, five ISO 25178-2 areal texture parameters *Sa, Sal, Sku, Ssk* and *Sq* were computed from the same topographies shown in Fig. 10. Differences in the areal texture parameters obtained using FVM, ICM, CSI and PAI from those obtained using AFM data are shown in Fig. 11. The authors acknowledge that areal texture parameters are often computed using topographies of larger sizes. However, in this study the largest area available for comparison was limited by the maximum measurement range (52 µm × 52 µm) of the AFM for the chosen sampling distance. As stated earlier, no band-pass filtering was applied to the topographies, thus the entire topographic content present at multiple scales contributed into defining the value of the texture parameters. In the case of FVM, texture parameters are computed using the replicated surface. The difference between the original and replicated surfaces may have contributed to the differences in the computed texture parameters. Based on the results shown in Fig. 11, CSI was found to provide *Sku* and *Ssk* values most similar to AFM, while PAI provided *Sa* and *Sq* values closest to AFM, and ICM provided *Sal* values closest to AFM. Overall, CSI was found to provide texture parameter values relatively close to AFM without significant difference in any of the five computed parameters. The differences in the *Sa* and *Sq* values obtained with CSI/ICM and AFM may be partly due to the form deviation between the topographies, which appeared in the form of bending at a spatial frequency of a few tens of micrometres. In such a case, the form of the topographies obtained with CSI and ICM were found to be in agreement. As stated in the introduction, being in consensus with AFM does not necessarily imply that CSI provided the best results. In absence of a reliable more accurate reference, the observation only indicates that a subset of technologies and setups (in this case, AFM and CSI) showed more agreement with each other, if compared to the other explored measurement solutions.

4. Conclusions

Optical measurement of surfaces can be very challenging, in particular when the surfaces are complex and novel, where no reference is available to verify the accuracy of the measurement. In such scenarios, a deeper insight and more comprehensive understanding of the performance and behaviour of current areal topography measurement solutions is necessary in order to improve confidence in the measured data. In this paper, the behaviour and performance of four different optical measurement technologies to characterise an optically challenging surface comprised of a top, thin transparent layer, were illustrated. In absence of a more accurate reference measurement method, the assessment of measurement performance and behaviour were performed based on consensus among topographies measured with multiple instruments. In order to reduce the risk of reaching the wrong consensus among instruments, additional sources of information (optical microscope imaging with focus stacking, scanning electron microscopy and atomic force microscopy) were selected. The results presented here have shown that measurement errors can be significant to the point that they may significantly alter the reconstructed topographies. The differences between topographies reconstructed from datasets achieved by means of different measurement technologies are visually appreciable, as demonstrated with the test case. In addition to visual inspection, quantitative comparison based on computing ISO 25178 areal texture parameters showed differences on the same order of magnitude. Granted, the test case was particularly challenging because it involved a transparent layer, particularly troublesome when optical measurement is involved, but other topographies, because of other intrinsic reasons for complexity, may be equally challenging. The computed texture parameters in the test case also showed that CSI is the technology that most closely approximates AFM results. It is worth noting that other instruments based on the same technologies as those investigated in this work, or the same instruments on different samples, may have different performance and behaviour, which can also be affected by other factors such as sub-optimal operating conditions, maintenance status and software version. This study is not aimed to determine which measurement technology or instrument is superior. But rather to show how easy it is to obtain significantly different results from the same surface when multiple instruments are applied to new surface types, and there have not been sufficient studies to investigate how the instruments behave with the specific surface, or to determine optimal measurement parameters. It is clear that most of the limitations revealed for the evaluated technologies stem from the material and optical properties of the sample. The focus of this study is to assess the behaviour of these optical measurement technologies for the specific application of measuring this type of challenging surface described in Section 2.1. The conclusions should be applicable to similar scenarios where a transparent film with complex surface topography is present on a substrate. However, it is worth noting that the thickness of the transparent layer in the test case is comparable to the peak-to-valley height variations on the surface. The authors expect further difficulties when measuring a film with a thickness much smaller than the peak-to-valley height variations on the surface. In conclusion we advise that each new surface should be carefully assessed, and measurement with multiple technologies should be attempted whenever possible. Also using more established means of investigation, such as SEM and AFM would be also advisable, whenever possible, as a means to acquire further information useful to establish a comparison reference, albeit quantitative is not always possible. We also conclude that there is an urgent need for more research into how to obtain traceability (and, therefore, measurement uncertainty) with such complex surfaces.

Acknowledgements

This work was supported by the Engineering and Physical Sciences Research Council [grant number EP/M008983/1] (EPSRC), Shanghai Jiao Tong University (grant numbers WF220502017 and WF102102003/030) and the European Metrology Programme for Innovation and Research (EMPIR) project FreeFORM (15SIB01). EMPIR is jointly funded by the EMPIR participating countries within EURAMET and the European Union. The authors would like to thank the Nanoscale and Microscale Research Centre (nmRC) at the University of Nottingham for providing access to SEM, and Dr Claudiu Giusca (Cranfield University) for providing access to the ICM instrument.

Supplementary materials

Supplementary material associated with this article can be found, in the online version, at doi:10.1016/j.optlaseng.2019.04.018.

References

[1] Thomas TR. Roughness and function. Surf Topog Met Props 2014;2:014001.
[2] Li YP, Li XY, Zhu XP, Lei MK, Lakhtakia A. Polymer surface textured with nanowire bundles to repel high-speed water drops. Langmuir 2018;34:5871–9.
[3] Bu L, Guo S, Zhang X, Shen X, Su D, Lu G, Zhu X, Yao J, Guo J, Huang X. Surface engineering of hierarchical platinum-cobalt nanowires for efficient electrocatalysis. Nat Commun 2016;7:11850.
[4] Chen H, Huang X, Zhang M, Damanik F, Baker MB, Leferink A, Yuan H, Truckenmüller R, van Blitterswijk C, Moroni L. Tailoring surface nanoroughness of electrospun scaffolds for skeletal tissue engineering. Acta Biomaterialia 2017;59:82–93.
[5] Kwok CT, Man HC, Cheng FT, Lo KH. Developments in laser-based surface engineering processes: with particular reference to protection against cavitation erosion. Surf Coat Technol 2016;291:189–204.
[6] Fleming RW. Visual perception of materials and their properties. Vision Res 2014;94:62–75.
[7] Bruzzone AAG, Costa HL, Lonardo PM, Lucca DA. Advances in engineered surfaces for functional performance. Ann CIRP 2008;57:750–69.
[8] Malshe AP, Bapat S, Rajurkar KP, Haitjema H. Bio-inspired textures for functional applications. Ann CIRP 2018;67:627–50.
[9] Leach RK. Optical measurement of surface topography. Berlin: Springer; 2011.
[10] International Organization for Standardization *ISO 25178-601:2010 Geometrical product specifications (GPS) – Surface texture: areal – Part 601: nominal characteristics of contact (stylus) instruments*.
[11] International Organization for Standardization *ISO 25178-602:2010 Geometrical product specifications (GPS) – Surface texture: areal – Part 602: nominal characteristics of non-contact (confocal chromatic probe) instruments*.
[12] International Organization for Standardization *ISO 25178-604:2013 Geometrical product specifications (GPS) – Surface texture: areal – Part 604: nominal characteristics of non-contact (coherence scanning interferometry) instruments*.
[13] International Organization for Standardization *ISO 25178-605:2014 Geometrical product specifications (GPS) – Surface texture: areal – Part 605: nominal characteristics of non-contact (point autofocus probe) instruments*.
[14] International Organization for Standardization *ISO 25178-606:2015 Geometrical product specification (GPS) – Surface texture: areal – Part 606: nominal characteristics of non-contact (focus variation) instruments*.
[15] International Organization for Standardization *ISO/FDIS 25178-600 Geometrical product specifications (GPS) – Surface texture: areal – Part 600: metrological characteristics for areal-topography measuring methods*.
[16] International Organization for Standardization *ISO/CD 25178-700 Geometrical product specification (GPS) – Surface texture: areal – Part 700: calibration, adjustment and verification of areal topography measuring instruments*.
[17] Leach RK, Giusca CL, Haitjema H, Evans C, Jiang X. Calibration and verification of areal surface texture measuring instruments. Ann CIRP 2015;64:797–813.
[18] Giusca CL, Leach RK. Calibration of the scales of areal surface topography measuring instruments: part 3. Resolution. Meas Sci Technol 2013;24:105010.
[19] Giusca CL, Leach RK, Helery F. Calibration of the scales of areal surface topography measuring instruments: part 2. Amplification, linearity and squareness. Meas Sci Technol 2012;23:065005.
[20] Giusca CL, Leach RK, Helary F, Gutauskas T, Nimishakavi L. Calibration of the scales of areal surface topography-measuring instruments: part 1. Measurement noise and residual flatness. Meas Sci Technol 2012;23:035008.
[21] Haitjema H, Morel MAA. Noise bias removal in profile measurements. Measurement 2005;38:21–9.
[22] de Groot PJ. The meaning and measure of vertical resolution in optical surface topography measurement. Appl Sci 2017;7:54.
[23] Maculotti G, Feng X, Galetto M, Leach RK. Noise evaluation of a point autofocus surface topography measuring instrument. Meas Sci Technol 2018;29:065008.
[24] Giusca CL, Claverley JD, Sun WJ, Leach RK, Helmli F, Chavigner MPJ. Practical estimation of measurement noise and flatness deviation on focus variation microscopes. Ann CIRP 2014;63:545–8.
[25] International Organization for Standardization *ISO 25178-603:2013 Geometrical product specifications (GPS) – Surface texture: areal – Part 603: nominal characteristics of non-contact (phase-shifting interferometric microscopy) instruments*.
[26] Blateyron F. Chromatic Confocal Microscopy. Optical measurement of surface topography. Leach RK, editor. Berlin, Heidelberg: Springer; 2011.
[27] Alburayt A, Syam WP, Leach R. Lateral scale calibration for focus variation microscopy. Meas Sci Technol 2018;29:065012.
[28] Leach RK, de Groot P, Haitjema H. Infidelity and the calibration of surface topography measuring instruments. In: Proc. ASPE, Las Vegas, USA Oct; 2018.
[29] Senin N, Thompson A, Leach RK. Characterisation of the topography of metal additive surface features with different measurement technologies. Meas Sci Technol 2017;28:095003.
[30] Thompson A, Senin N, Giusca C, Leach R. Topography of selectively laser melted surfaces: a comparison of different measurement methods. Ann CIRP 2017;66:543–6.
[31] Leach R, Haitjema H. Bandwidth characteristics and comparisons of surface texture measuring instruments. Meas Sci Technol 2010;21:032001.
[32] Sang Myung L, Dongseok S, Ilgu Y. Characterization methodology of transparent hard coating film on transparent substrates using capacitance-voltage measurement. In: Proc. ICEP; 2016. p. 145–8.
[33] Kim D, Kim S, Kong HJ, Lee Y. Measurement of the thickness profile of a transparent thin film deposited upon a pattern structure with an acousto-optic tunable filter. Opt Lett 2002;27:1893–5.
[34] Kwon S, Kim N, Jo T, Pahk HJ. Critical dimension measurement of transparent film layers by multispectral imaging. Opt Express 2014;22:17370–81.
[35] International Organization for Standardization *ISO 25178-2:2012 Geometrical product specifications (GPS) – Surface texture: areal – Part 2: terms, definitions and surface texture parameters*.
[36] Blateyron F. The areal field parameters. Characterisation of areal surface texture. Leach RK, editor. Berlin: Springer; 2013.
[37] Adelson EH, Anderson CH, Bergen JR, Burt PJ, Ogden JM. Pyramid methods in image processing. RCA Eng 1984;29:33–41.
[38] Groot PJd, Lega XCd, Fay MF. Transparent film profiling and analysis by interference microscopy. Proc SPIE Opt Eng Appl 2008;7064:70640I.
[39] de Groot P. Principles of interference microscopy for the measurement of surface topography. Adv Opt Photon 2015;7:1–65.
[40] Larkin KG. Efficient nonlinear algorithm for envelope detection in white light interferometry. J Opt Soc Am A 1996;13:832–43.
[41] Digital Surf 2018 Mountains® surface imaging & metrology software Available: http://www.digitalsurf.com/en/mntkey.html (Accessed 18 May 2018).
[42] Besl PJ, McKay ND. A method for registration of 3-D shapes. IEEE Trans Pattern Anal Mach Intell 1992;14:239–56.
[43] Ekberg P, Su R, Leach R. High-precision lateral distortion measurement and correction in coherence scanning interferometry using an arbitrary surface. Opt Express 2017;25:18703–12.
[44] Feng X, Pascal J, Lawes S. A microscopy approach for in situ inspection of micro-coordinate measurement machine styli for contamination. Meas Sci Technol 2017;28:095010.
[45] Goodall RH, Darras LP, Purnell MA. Accuracy and precision of silicon based impression media for quantitative areal texture analysis. Sci Rep 2015;5:10800.
[46] Artigas R. Imaging confocal microscopy. Optical measurement of surface topography. Leach R, editor. Berlin: Springer; 2011.